arXiv:1001.0022v1 [hep-ph] 4 Jan 2010

$\mu\tau$ Production at Hadron Colliders

Tao Han,[*] **Ian Lewis**[†]

Department of Physics, University of Wisconsin, Madison, WI 53706, U.S.A.

Marc Sher[‡]

Particle Theory Group, College of William and Mary, Williamsburg, Virginia 23187

ABSTRACT: Motivated by large $\nu_\mu - \nu_\tau$ flavor mixing, we consider $\mu\tau$ production at hadron colliders via dimension-6 effective operators, which can be attributed to new physics in the flavor sector at a higher scale Λ. Current bounds on many of these operators from low energy experiments are very weak or nonexistent, and they may lead to clean $\mu^+\tau^-$ and $\mu^-\tau^+$ signals at hadron colliders. At the Tevatron with 8 fb^{-1}, one can exceed current bounds for most operators, with most 2σ sensitivities being in the $6-24$ TeV range. We find that at the LHC with 1 fb^{-1} (100 fb^{-1}) integrated luminosity, one can reach a 2σ sensitivity for $\Lambda \sim 3-10$ TeV ($\Lambda \sim 6-21$ TeV), depending on the Lorentz structure of the operator. For some operators, an improvement of several orders of magnitude in sensitivity can be obtained with only a few tens of pb^{-1} at the LHC.

KEYWORDS: Lepton flavor physics; Hadron collider phenomenology..

[*]than@hep.wisc.edu
[†]ilewis@wisc.edu
[‡]mtsher@wm.edu

Contents

1. Introduction

The most important discovery in particle physics in the past decade has only deepened the mystery of "flavor" of quarks and leptons. The fact that the mixing angles in the leptonic sector are large [1, 2] stands in sharp contrast with the observed small mixing angles in the quark sector. In particular, mixing between the second and third generation neutrinos appears to be maximal. Of course, this large mixing could occur from diagonalizing the neutrino mass matrix, the charged lepton mass matrix, or both. At present, the source of this large mixing is a mystery.

In view of this, it is tempting to explore other interactions which change lepton flavor between the second and third generations. Several years ago, two of us (TH, MS), along with Black and He (BHHS) [3], performed a comprehensive analysis of constraints on these interactions based on low energy meson physics. BHHS chose an effective field theory approach, in which all dimension-6 operators of the form

$$(\bar{\mu}\,\Gamma\,\tau)\,(\bar{q}^{\alpha}\,\Gamma\,q^{\beta})\,, \tag{1.1}$$

were studied, where Γ contains possible Dirac γ-matrices. With six flavors of quarks, there were 12 possible combinations of q^a and q^b (assuming Hermiticity), six diagonal and six off-diagonal, and four choices S, P, V, A of the gamma matrices were considered. All of these operators were considered, and most were bounded by considering τ, K, B and t decays.

In particular, BHHS considered operators of the form

$$\Delta\mathcal{L} = \Delta\mathcal{L}_{\tau\mu}^{(6)} = \sum_{j,\alpha,\beta} \frac{\mathcal{C}_{\alpha\beta}^j}{\Lambda^2} \left(\overline{\mu}\,\Gamma_j\,\tau\right)\left(\overline{q}^\alpha\,\Gamma_j\,q^\beta\right) + \text{H.c.}\,, \tag{1.2}$$

where $\Gamma_j \in (1, \gamma_5, \gamma_\sigma, \gamma_\sigma\gamma_5)$ denotes relevant Dirac matrices, specifying scalar, pseudoscalar, vector and axial vector couplings, respectively. They did not consider tensor operators since the hadronic matrix elements were not known and the bounds were expected to be weak in any event. They chose a value of

$$\mathcal{C}_{\alpha\beta}^j \;=\; 4\pi\,\mathcal{O}(1) \qquad (\text{default})\,, \tag{1.3}$$

which corresponds to an underlying theory with a strong gauge coupling of $\alpha_S = \mathcal{O}(1)$. Arguments can be made for multiplying or dividing this by 4π, for naive dimensional analysis or for weakly coupled theories, respectively. A discussion is found in BHHS; we simply choose the above definition of Λ and other choices can be made by simple rescaling.

BHHS found that operators involving the three lightest quarks were strongly bounded, with bounds ranging from 3 to 13 TeV on the related value of Λ. These bounds can be found in Appendix A. Not surprisingly, operators involving the top quark were either unbounded or very weakly bounded, with only the $\overline{t}u$ operator for vector and axial vector couplings being bounded by $\Lambda < 650$ GeV (the bound arises through a loop in $B \to \mu\tau$ decay). Operators involving the b-quark and a light quark also have bounds on Λ which were generally in the several TeV range. However, there were some surprises. The scalar and pseudoscalar operators involving $\overline{c}u$ and $\overline{c}c$ were completely unbounded, and the $\overline{b}b$ operator was essentially unbounded for all S, P, V, A operators. And, as noted above, **none** of the tensor operators were considered at all, for all quark combinations.

In this note, we point out that the operators in Eq. (1.1) (without involving top quarks) will contribute to $\mu - \tau$ production at hadron colliders. Given that many of the possible operators, as noted above, are completely unbounded or weakly bounded from the current low energy data, study of $pp \to \mu\tau$ at the LHC or $p\overline{p} \to \mu\tau$ at the Tevatron will probe unexplored territory. There have been some previous discussions of $\mu - \tau$ production at hadron colliders. Han and Marfatia [4] looked at the lepton-violating decay $h \to \mu\tau$ at hadron colliders, and a very detailed analysis of signals and backgrounds was carried out by Assamagan et al. [5] afterwards. Other work looking at Higgs decays focused on mirror fermions [6], in supersymmetric models [7], in seesaw neutrino models [8], and in Randall-Sundrum models [9]. In addition to Higgs decays, others have considered lepton-flavor violation in the decays of supersymmetric particles [10] and in horizontal gauge boson models [11]. These analyses, however, were done in the context of very specific models (often relying on the assumption

that the μ and τ are emitted in the decay of a single particle). Here, we will use a much more general effective field theory approach.

This paper is organized as follows. In the next section, we discuss the cross sections for $\mu\tau$ production via the various operators. A detailed analysis of the signal identification and background subtraction is in Section 3, and Section 4 contains some discussions and our conclusions. Appendix A reiterates the bounds from BHHS for comparison, and Appendix B outlines the calculation of partial-wave unitarity bounds.

2. $\mu\tau$ Production at Hadron Colliders

Due to the absence of the appreciable $\mu\tau$ production in the SM, their production can be estimated via the effective operators in Eq. (1.1). On dimensional grounds, the cross section for $\bar{q}_i q_j \to \mu\tau$ grows with center of mass energy, i.e.,

$$\sigma(\bar{q}_i q_j \to \mu\tau) \propto \frac{s}{\Lambda^4}, \tag{2.1}$$

where $\sqrt{s}$ is the center of mass energy for the partonic system. This growth of cross section with energy will eventually violate unitarity bounds. Expanding the scattering amplitudes in partial waves, we find the unitarity bounds to be (see Appendix B)

$$s \leq \begin{cases} 2\Lambda^2 \text{ for scalar, pseudoscalar, and tensor;} \\ 3\Lambda^2 \text{ vector and axial vector case.} \end{cases} \tag{2.2}$$

The total cross sections for $\mu\tau$ production at the hadronic level after convoluting with the parton distribution functions (pdfs) are

$$\sigma_{\text{Scalar}} = \frac{\pi}{3} \frac{S}{\Lambda^4} \int_{\tau_0}^{\tau_{\text{max}}} d\tau (q \otimes q)(\tau) \left(1 - \frac{\tau_0}{\tau}\right)^2 \tau \tag{2.3}$$

$$\sigma_{\text{Vector}} = \frac{4\pi}{9} \frac{S}{\Lambda^4} \int_{\tau_0}^{\tau_{\text{max}}} d\tau (q \otimes q)(\tau) \left(1 - \frac{\tau_0}{\tau}\right)^2 \left(1 + \frac{\tau_0}{2\tau}\right) \tau \tag{2.4}$$

$$\sigma_{\text{Tensor}} = \frac{8\pi}{9} \frac{S}{\Lambda^4} \int_{\tau_0}^{\tau_{\text{max}}} d\tau (q \otimes q)(\tau) \left(1 - \frac{\tau_0}{\tau}\right)^2 \left(1 + 2\frac{\tau_0}{\tau}\right) \tau. \tag{2.5}$$

The pseudoscalar cross section is of the same form as the scalar cross section, and the axial vector cross section is of the same form as the vector cross section. Our perturbative calculation will become invalid at the unitarity bound, hence there is a maximum on the τ integration. It is given by $\tau_{\text{max}} = 2\Lambda^2/S$ for the scalar, pseudoscalar, and tensor cases, $\tau_{\text{max}} = 3\Lambda^2/S$ for the vector and axial-vector cases, $\tau = \hat{s}/S$, $\tau_0 = m_\tau^2/S$, m_τ is the tau mass, and S is the center of mass energy in the lab frame. Also, $q(x)$ is the quark distribution function with flavor sum suppressed, and $\otimes$ denotes the convolution defined as

$$(g_1 \otimes g_2)(y) = \int_0^1 dx_1 \int_0^1 dx_2 \, g_1(x_1) g_2(x_2) \delta(x_1 x_2 - y). \tag{2.6}$$

Table 1: Cross sections for all the scalar, vector, and tensor structures at the Tevatron at 2 TeV, the LHC at 10 TeV, and the LHC at 14 TeV. The pseudoscalar (axial vector) cross section is the same as the scalar (vector) cross section. All cross sections were evaluated with $\Lambda = 2$ TeV.

σ (pb)	Tevatron 2 TeV ($p\bar{p}$)			LHC 10 TeV (pp)			LHC 14 TeV (pp)		
	$1,\gamma_5$	$\gamma_\mu,\gamma_\mu\gamma_5$	$\sigma_{\mu\nu}$	$1,\gamma_5$	$\gamma_\mu,\gamma_\mu\gamma_5$	$\sigma_{\mu\nu}$	$1,\gamma_5$	$\gamma_\mu,\gamma_\mu\gamma_5$	$\sigma_{\mu\nu}$
$u\bar{u}$	8.4	11	22	63	85	170	120	160	310
$d\bar{d}$	2.5	3.3	6.7	38	51	100	72	98	190
$s\bar{s}$	0.18	0.24	0.49	5.5	7.4	15	11	15	30
$d\bar{s}$	1.3	1.7	3.4	34	45	91	66	89	180
$d\bar{b}$	0.50	0.67	1.3	17	22	45	34	46	90
$s\bar{b}$	0.13	0.17	0.34	5.0	6.7	13	11	14	28
$u\bar{c}$	1.5	2.0	3.9	41	55	110	80	110	210
$c\bar{c}$	0.070	0.094	0.19	2.6	3.5	7.0	5.5	7.3	15
$b\bar{b}$	0.021	0.028	0.056	1.1	1.5	2.9	2.4	3.2	6.4

The CTEQ6L parton distributution function set is used for all of the results [12].

Results for the cross sections for the scalar, pseudoscalar, vector, axial vector, and tensor structures at the Tevatron, LHC at 10 TeV and 14 TeV are given in Table 1. The cross section for the pseudoscalar (axial vector) current is the same as for the scalar (vector) current. For all cases, Λ is set equal to 2 TeV and the unitarity bounds are taken into consideration. At this rather high scale, the production rates are dominated by the valence quark contributions. The cross sections at the LHC are larger than those at the Tevatron by roughly an order of magnitude, reaching about 100 pb.

For some cases the bounds from BHHS are greater than 2 TeV, hence the cross section needs to be scaled to determine a realistic cross section at hadron colliders. The partonic cross sections scale at Λ^{-4}, but at the hadronic level a complication arises since the unitarity bounds introduce a dependence on the new physics scale in the integration over pdfs. If the unitarity bounds are ignored ($\tau_{\max} = 1$), one finds that with $\Lambda = 2$ TeV neglecting the unitarity bounds has at most a 10% effect on the cross sections at the LHC for both 10 TeV and 14 TeV and no effect at the Tevatron since the unitarity bounds are greater than the lab frame energy. Hence, if Λ is increased from 2 TeV, at the LHC it is a good approximation to assume the cross section scales as Λ^{-4} and at the Tevatron the cross section scales exactly as Λ^{-4}. For example, the lower bound on Λ for the vector $u\bar{u}$ coupling from BHHS is 12 TeV, so the maximum cross section at the 14 TeV LHC from this operator would be approximately $160 \times (2/12)^4$ pb $= 120$ fb. On the other hand, there is no bound whatsoever for the vector $u\bar{c}$ coupling, and thus a cross section limit of 110 pb would yield a new limit of 2 TeV on the scale of this operator. This would constitute an improvement of many orders of magnitude.

3. Signal Identification and Backgrounds

Upon production at hadron colliders, τ's will promptly decay and are detected via their decay products. About 35% of the time the τ decays to two neutrinos and an electron or muon, the other 65% of the time the τ decays to a few hadrons plus a neutrino. We will consider the τ decay to an electron as well as hadronic decays in this work. The decay to a muon will result in a $\mu^+\mu^-$ final state that has a large Drell-Yan background. We will study the signal reach at the Tevatron and at the 14 TeV LHC.

3.1 τ Decay to Electrons

3.1.1 Signal Reconstruction

The τ decays to an electron plus two neutrinos about 18% of the time. We thus search for a final state of an electron and muon

$$e + \mu. \tag{3.1}$$

The electromagnetic calorimeter resolution is simulated by smearing the electron energies according to a Gaussian distribution with a resolution parameterized by

$$\frac{\sigma(E)}{E} = \frac{a}{\sqrt{E/\text{GeV}}} \oplus b, \tag{3.2}$$

where the constants are $a = 10\%$ and $b = 0\%$ at the Tevatron [13], $a = 5\%$ and $b = 0.55\%$ at the LHC [14], and $\oplus$ indicates addition in quadrature. For simplicity, we have used the same form of smearing for the muons.

The decay of the τ leaves us with some missing energy and we need to consider how to effectively reconstruct the τ momentum. For our process all the missing transverse momentum is coming from the τ, hence

$$\mathbf{p}_T^\tau = \mathbf{p}_T^e + \mathbf{p}_T^{\text{miss}}. \tag{3.3}$$

At hadron colliders, we have no information on the longitudinal component of the missing momentum on an event-by-event basis. However, the τ will be highly boosted and its decay products will be collimated. Hence, the missing momentum should be aligned with the electron momentum and the ratio p_z^e/p_z^{miss} should be the same as the ratio of the magnitudes of the transverse momenta, p_T^e/p_T^{miss}. Therefore, the longitudinal component of the τ can be reconstructed as [4]

$$p_z^\tau = p_z^e \left(1 + \frac{p_T^{\text{miss}}}{p_T^e} \right). \tag{3.4}$$

Once the three-momentum is reconstructed, we can solve for the τ energy, $E_\tau^2 = \mathbf{p}_\tau^2 + m_\tau^2$. Figure 1 illustrates the effectiveness of this method at the Tevatron. Figure 1(a) (Figure 1(b)) shows the transverse momentum (longitudinal mometum) distribution for the theoretically

generated (solid) and kinematically reconstructed (dashed) τ momenta. As can be seen, the τ momentum is reconstructed effectively.

We first apply some basic cuts on the transverse momentum and the pseudo rapidity to simulate the detector acceptance and triggering, as well as to isolate the signal from the background,

$$
\begin{aligned}
p_T^\mu > 20 \text{ GeV}, \qquad |\eta^\mu| < 2.5, \\
p_T^e > 20 \text{ GeV}, \qquad |\eta^e| < 2.5.
\end{aligned}
\tag{3.5}
$$

Since the signal does not contain any jets, we also require a jet veto such that there are no jets with $p_T > 50$ GeV and $|\eta| < 2.5$.

There are several distinctive kinematic features of our signal. The decay products of the τ will be highly collimated, and the electron transverse momentum will be traveling in the same direction as the missing transverse momentum. Also, in the transverse plane the muon and tau should be back to back. Since the electron will mostly be in the direction of the τ, it will also be nearly back to back with the muon. Finally, the τ and μ have equal transverse momenta; hence, the decay products of the τ have less transverse momentum than the μ. We can measure this discrepancy using the momentum imbalance

$$
\Delta p_T = p_T^\mu - p_T^e.
\tag{3.6}
$$

For the signal, this observable should be positive. Based on the kinematics of our signal, we apply the further cuts [5]

$$
\begin{aligned}
\delta\phi(p_T^\mu, p_T^e) > 2.75 \text{ rad}, \qquad \delta\phi(p_T^{\text{miss}}, p_T^e) < 0.6 \text{ rad}, \\
\Delta p_T > 0.
\end{aligned}
\tag{3.7}
$$

3.1.2 Backgrounds and their Suppression

The leading backgrounds are W^+W^- pair production, $Z^0/\gamma^\star \to \tau^+\tau^-$, and $t\bar{t}$ pair production [5]. The total rates for these backgrounds at the Tevatron and the LHC are given in Table 2 with consecutive cuts. We consider both of the final states with μ^+ and μ^-.

The partonic cross section of our signal increases with energy while the cross sections of the backgrounds will decrease with energy. Hence, the invariant mass distribution of our signal does not fall off as quickly as the backgrounds.

Figure 2(a) shows the invariant mass distributions of backgrounds and our signal at the Tevatron with initial states $c\bar{c}$ and $u\bar{c}$ with various couplings and a new physics scale of 1 TeV after applying the cuts in Eqs. (3.5) and (3.7). The cross section for the pseudoscalar (axial-vector) couplings are the same as those for the scalar (vector) couplings. The decline in the signal rates is due to a suppression of the pdfs at large x. Although the signal rates steeply decline with invariant mass the background falls off faster. The $u\bar{c}$ signal is still clearly above background due to a valence quark in the initial state, but the $c\bar{c}$ signal distribution is
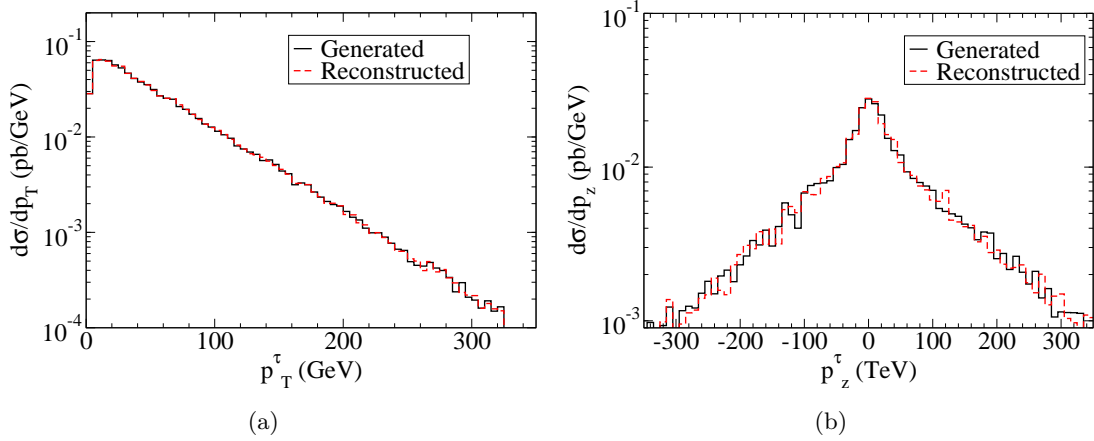
Figure 1: The distributions of the transverse momentum of the generated and reconstructed τ momentum, (a) for the distribution of the magnitude τ transverse momentum and (b) for the distribution of the magnitude of the τ longitudinal momentum.

Table 2: Backgrounds to the τ's electronic decay before and after cuts at (a) the Tevatron and (b) the LHC.

Backgrounds (pb)	No Cuts	Cuts Eq. (3.5)	+ Eq. (3.7)	+ Eq. (3.8)
(a) Tevatron 2 TeV				
$W^+W^- \to \mu^\pm \nu_\mu \tau^\mp \nu_\tau$	0.032	0.0046	0.0012	2.6×10^{-4}
$W^+W^- \to \mu^\pm \nu_\mu e^\mp \nu_e$	0.18	0.13	0.0060	9.8×10^{-4}
$Z^0/\gamma^\star \to \tau^+\tau^- \to \mu^\pm \nu_\mu \tau^\mp$	610	0.21	0.091	1.4×10^{-4}
$t\bar{t} \to \mu^\pm \nu_\mu b \tau^\mp \nu_\tau \bar{b}$	0.020	6.5×10^{-4}	7.4×10^{-5}	4.4×10^{-5}
$t\bar{t} \to \mu^\pm \nu_\mu b e^\mp \nu_e \bar{b}$	0.11	0.0099	7.3×10^{-4}	2.7×10^{-4}
(b) LHC 14 TeV				
$W^+W^- \to \mu^\pm \nu_\mu \tau^\mp \nu_\tau$	0.34	0.030	0.0088	0.0031
$W^+W^- \to \mu^\pm \nu_\mu e^\mp \nu_e$	1.9	0.99	0.051	0.014
$Z^0/\gamma^\star \to \tau^+\tau^- \to \mu^\pm \nu_\mu \tau^\mp$	2300	1.1	0.49	0.0014
$t\bar{t} \to \mu^\pm \nu_\mu b \tau^\mp \nu_\tau \bar{b}$	1.9	0.070	0.010	0.0077
$t\bar{t} \to \mu^\pm \nu_\mu b e^\mp \nu_e \bar{b}$	11	1.5	0.10	0.050

much closer to the background distribution due to the steep fall with invariant mass and a lack of an initial state valence quarks. Figure 2(b) shows the invariant mass distributions of backgrounds and our signal at the Tevatron with initial state $u\bar{c}$ and scalar coupling for various new physics scales. The 3 TeV new physics scale invariant mass distribution is approaching the background distribution. A higher cutoff on the invariant mass will be needed to separate the weak signal from the backgrounds. Based on Fig. 2, we propose a selection cut on

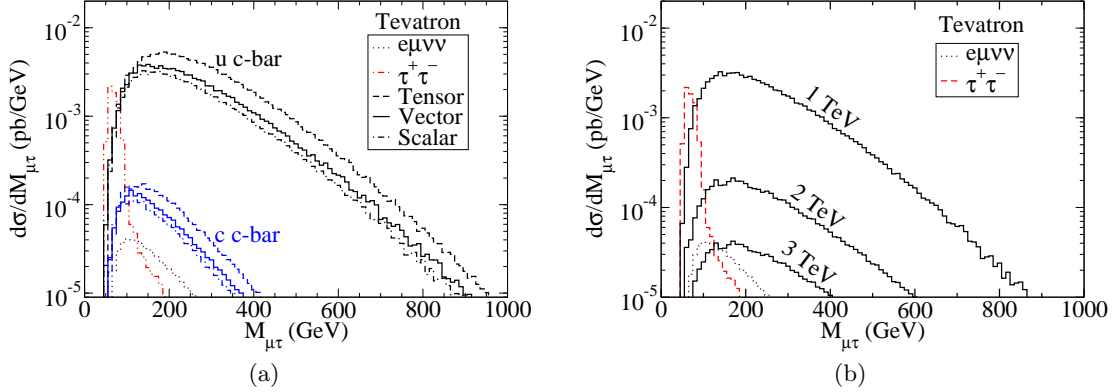$$M_{\mu\tau} > 250 \text{ GeV}. \tag{3.8}$$

Figure 2: The distributions of the invariant mass of the reconstructed $\tau - \mu$ system for signal and background at the Tevatron, (a) for the invariant mass distribution for the $u\bar{c}$ and $c\bar{c}$ initial states and a new physics scale of 1 TeV for our signal, and (b) for the invariant mass distribution for various new physics scales for our signal with $u\bar{c}$ initial state.

Table 2 shows the effects of the invariant mass cut on the backgrounds in the last column.

Similar analyses can be carried out for the LHC. Figure 3(a) shows the invariant mass distribution for our signal with the $u\bar{c}$ and $c\bar{c}$ initial states and various Lorentz structures, as well as the backgrounds after the cuts in Eqs. (3.5) and (3.7). The new physics scale was set to 1 TeV and the unitarity bound is imposed. Figure 3(b) shows the invariant mass distribution of the $u\bar{c}$ initial state with various new physics scales. The cutoff on the invariant mass corresponds to the unitarity bound, the scale at which the perturbative calculation becomes untrustworthy. In the lack of the knowledge for the new physics to show up at the scale Λ, we simply impose a sharp cutoff at the unitarity bound. As compared with the Tevatron, the LHC signal rates fall off much less quickly with invariant mass since the Tevatron's lower energy leads to a suppression from the pdfs at large x. As can be seen, as the new physics scale increases the cross section decreases and the background becomes more problematic at lower invariant mass. Also, as the new physics scale increases the unitarity bound becomes less strict. Hence, although the backgrounds at the LHC are considerably larger than at the Tevatron, for large new physics scales the LHC has an enhancement in the signal cross section from the large invariant mass region.

3.2 τ Decay to Hadrons

Although with significantly larger backgrounds, the signal from τ hadronic decays can be very distinctive as well. We limit the hadronic τ decays to 1-prong decays to pions, i.e., $\tau^{\pm} \to \pi^{\pm}\nu_{\tau}$, $\tau^{\pm} \to \pi^{\pm}\pi^0\nu_{\tau}$, and $\tau^{\pm} \to \pi^{\pm}2\pi^0\nu_{\tau}$. The τ's have 1-prong decays to these final states about 50% of the time. We thus search for a final state of a τ jet and a muon
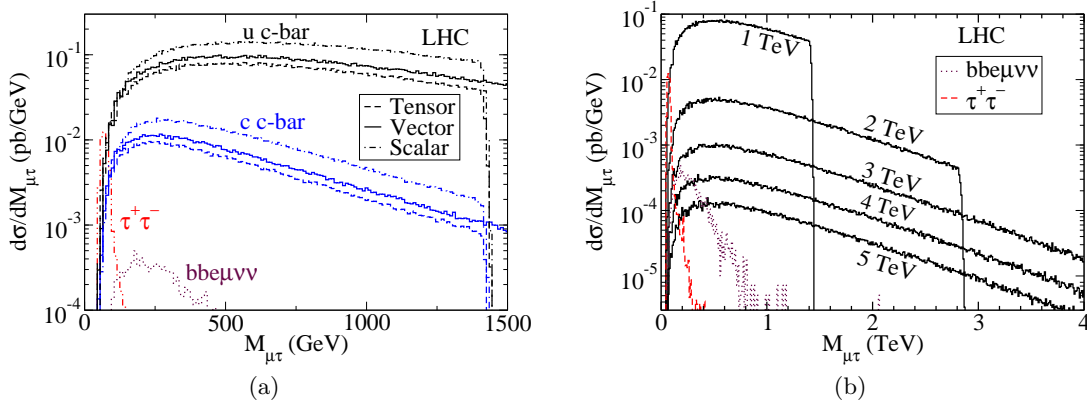
$$j_{\tau} + \mu. \tag{3.9}$$

Figure 3: The distributions of the invariant mass of the reconstructed $\tau - \mu$ system for signal and background at the LHC, (a) for the invariant mass distribution for the $u\bar{c}$ and $c\bar{c}$ initial states and a new physics scale of 1 TeV for our signal, and (b) for the invariant mass distribution for various new physics scales for our signal with $u\bar{c}$ initial state.

To simulate detector resolution effects, the energy is smeared according to Eq. (3.2) with $a = 80\%$ and $b = 0\%$ for the jet at the Tevatron. As in the electronic decay, the τ is highly boosted and its decay products are collimated. Hence, all the missing energy in the event should be aligned with the τ. The signal is then reconstructed as described in Eqs. (3.3) and (3.4) with the electron momentum replaced by the momentum of the τ-jet.

The hadronic decay of the τ also has the backgrounds W^+W^- pair production, $Z^0/\gamma^\star \to \tau^+\tau^-$, and $t\bar{t}$ pair production plus an additional background of W+jet, where the jet is misidentified as a τ-jet. At the Tevatron, we assume a τ-jet tagging efficiency of 67% and that a light jet is mistagged as a τ-jet 1.1% of the time [15]. Even with a low rate of misidentification, the W+jet background is large. To suppress this background, we note that for hadronic decays most of the τ transverse momentum will be carried by the jet. Hence the τ-jet should be traveling in the same direction as the reconstructed τ momentum. Motivated by this observation, we apply the same cuts as Eqs. (3.5), (3.7), and (3.8) with the electron momentum replaced by the τ-jet momentum and the additional cuts

$$\frac{p_T^{\tau-jet}}{p_T^\tau} > 0.6 \qquad\qquad \Delta R(p_T^{\tau-jet}, p^\tau) > 0.2 \text{ rad.} \qquad (3.10)$$

3.3 Sensitivity Reach at the Tevatron

One can determine the sensitivity of the Tevatron to the new physics scale with 8 fb^{-1} of data. Table 3 shows the sensitivity of the Tevatron for (a) electronic and (b) hadronic τ decays. The tables list the maximum new physics scale sensitive at 2σ and 5σ level at the Tevatron. The reaches for scalar (vector) and pseudoscalar (axial-vector) are the same at the Tevatron, although the previous bounds from BHHS for the scalar (vector) and pseudoscalar (axial-vector) couplings may not be the same. The bounds from BHHS can be found in

Appendix A. If only one of the bounds for scalar (vector) or pseudoscalar (axial-vector) coupling from BHHS is greater than the Tevatron reach one star is placed next to the new physics scale, if both bounds are greater than the Tevatron reach two stars are places next to the new physics scale. Due to the larger backgrounds from W+jet, the Tevatron is much less sensitive to the τ hadronic decays than the τ electronic decays.

There were no bounds from BHHS for the tensor couplings, so the Tevatron will be able to exlude some of the parameter space. Since the tensor cross sections are generally at least twice as large as the scalar cross sections, the Tevatron is more sensitive to the tensor couplings than it is to scalar couplings. Also, in general, the Tevatron is more sensitive to processes with initial state valence quarks than those without initial state quarks. With 8 fb^{-1} of data most of the bounds can be increased, some quite stringently.

Somewhat similar leptonic final states have been searched for in a model-independent way at the Tevatron [16], although these included substantial missing energy and possible jets. We encourage the Tevatron experimenters to carry out the analyses as suggested in this article.

3.4 Sensitivity Reach at the LHC

The LHC is also sensitive to flavor changing operators. For the signal and background analysis, we used the same kinematical cuts as we used at the Tevatron, see Eqs. (3.5), (3.7), and (3.8). Table 4 shows the sensitivity of the LHC to all possible initial states and the couplings under consideration with 100 fb^{-1} of data. The table contains the maximum new physics scales sensitive at 2σ and 5σ level at the LHC. As with the Tevatron, the LHC reach for scalar (vector) couplings is the same as that for pseudoscalar (axial-vector) couplings, although the bounds from BHHS may be different. If only one of the bounds for scalar (vector) or pseudoscalar (axial-vector) coupling from BHHS is greater than the LHC reach one star is placed next to the new physics scale, if both bounds are greater than the LHC reach two stars are placed next to the new physics scale. Despite the larger backrounds for the hadronic τ decays, at the LHC the reaches for the hadronic and electronic τ decays are much more similar than at the Tevatron since the LHC cross section receives an enhancement from the large invariant mass region. For electronic (hadronic) τ decays the LHC with 100 fb^{-1} of data is less (more) sensitive than the Tevatron with 8 fb^{-1} of data.

Figure 4 shows the integrated luminosities needed for the sensitivity at the LHC to various initial states with τ decay to electrons as a function of the new physics scale. For some initial states and Lorentz structures BHHS had a bound on the new physics scale larger than 1 TeV. In those cases the distribution does not begin until the bound on the new physics scale. The sensitivity for the pseudoscalar (axial-vector) is the same as the scalar (vector) state, although the bounds from BHHS are different. Note that extraordinary improvement in the bounds could be found (or a discovery made) with relatively low integrated luminosity. Consider, for example, the $u\bar{c}$ initial state. There is currently no bound at all; in principle, Λ could be tens of GeV. The figure shows that a total integrated luminosity of an inverse picobarn would give

Table 3: New physics scale sensitive at 2σ and 5σ level at the Tevatron with 8 fb^{-1} of data, (a) for τ electronic decay and (b) for hadronic decay. One star indicates that the Tevatron reach is less than one of the scalar (vector) or pseudoscalars (axial-vector) bounds from BHHS, and two stars indicates that the Tevatron reach is less than both bounds from BHHS.

(a) $\tau \to e$						
$\Lambda_{\rm NP}$ (TeV)	2σ sensitivity			5σ discovery		
Coupling	$1,\gamma_5$	$\gamma_\mu,\gamma_\mu\gamma_5$	$\sigma_{\mu\nu}$	$1,\gamma_5$	$\gamma_\mu,\gamma_\mu\gamma_5$	$\sigma_{\mu\nu}$
$u\bar{u}$	20	21	24	14	15	17
$d\bar{d}$	17	18	21	12	13	15
$s\bar{s}$	9.9	10	12	7.2*	7.7**	8.7
$d\bar{s}$	15	16	18	10	11*	13
$d\bar{b}$	13	14	16	9.8	10*	11
$s\bar{b}$	9.5	10	11	6.9	7.3	8.3
$u\bar{c}$	17	18	20	12	13	14
$c\bar{c}$	7.9	8.3	9.5	5.7	6.0	6.9
$b\bar{b}$	6.4	6.8	7.7	4.6	4.9	5.6
(b) $\tau \to h^{\pm}$						
$\Lambda_{\rm NP}$ (TeV)	2σ sensitivity			5σ discovery		
Coupling	$1,\gamma_5$	$\gamma_\mu,\gamma_\mu\gamma_5$	$\sigma_{\mu\nu}$	$1,\gamma_5$	$\gamma_\mu,\gamma_\mu\gamma_5$	$\sigma_{\mu\nu}$
$u\bar{u}$	8.6**	9.2**	10	6.5**	6.9**	8.1
$d\bar{d}$	5.7**	6.1**	7.1	4.3**	4.6**	5.4
$s\bar{s}$	1.8*	1.9**	2.3	1.4**	1.4**	1.7
$d\bar{s}$	3.7	4.0*	4.6	2.8*	3.0**	3.5
$d\bar{b}$	2.7*	2.9*	3.4	2.0**	2.2	2.5
$s\bar{b}$	1.5**	1.6**	1.9	1.1**	1.2**	1.4
$u\bar{c}$	3.9	4.1	4.8	2.9	3.1	3.6
$c\bar{c}$	1.1	1.2	1.4	0.89	0.95**	1.1
$b\bar{b}$	0.91	0.97	1.1	0.68	0.73	0.86

a 5σ sensitivity for a Λ of 1 TeV. An integrated luminosity of an inverse femtobarn would give substantial improvements for all of the operators shown in Fig. 4.

4. Discussions and Conclusions

In a previous article, motivated by discovery of large $\nu_\mu - \nu_\tau$ mixing in charged current interactions, bounds on the analogous mixing in neutral current interactions were explored. A general formalism for dimension-6 fermionic effective operators involving $\tau - \mu$ mixing with typical Lorentz structure $(\overline{\mu}\Gamma\tau)(\overline{q}^\alpha\Gamma q^\beta)$ was presented, and the low-energy constraints on the new physics scale associated with each operator were derived, mostly from experimental

Table 4: New physics scale sensitive at 2σ and 5σ level at the LHC with 100 fb^{-1} of data, (a) for τ electronic decay and (b) for hadronic decay. One star indicates that the LHC reach is less than one of the scalar (vector) or pseudoscalars (axial-vector) bounds from BHHS, and two stars indicates that the LHC reach is less than both bounds from BHHS.

(a) $\tau \to e$						
Λ_{NP} (TeV)	2σ sensitivity			5σ discovery		
Coupling	$1,\gamma_5$	$\gamma_\mu,\gamma_\mu\gamma_5$	$\sigma_{\mu\nu}$	$1,\gamma_5$	$\gamma_\mu,\gamma_\mu\gamma_5$	$\sigma_{\mu\nu}$
$u\bar{u}$	18	19	21	14	15	17
$d\bar{d}$	16	17	19	12	13	15
$s\bar{s}$	9.0*	9.6*	11	7.1*	7.6**	8.6
$d\bar{s}$	13	14	16	10	11*	13
$d\bar{b}$	12	13	14	9.7	10	11
$s\bar{b}$	8.7	9.2	10	6.8	7.3	8.2
$u\bar{c}$	15	16	18	12	13	14
$c\bar{c}$	7.2	7.6	8.6	5.7	6.0	6.8
$b\bar{b}$	5.8	6.2	7.0	4.6	4.9	5.5
(b) $\tau \to h^{\pm}$						
Λ_{NP} (TeV)	2σ sensitivity			5σ discovery		
$u\bar{u}$	15	16	18	12	13	14
$d\bar{d}$	13	14	16	10*	11*	13
$s\bar{s}$	7.9*	8.4**	9.7	6.2*	6.7**	7.7
$d\bar{s}$	11	12*	14	9.3	9.9*	11
$d\bar{b}$	10	11	13	8.4*	8.9	10
$s\bar{b}$	7.6	8.1	9.3	6.0	6.4	7.4
$u\bar{c}$	13	14	16	10	11	12
$c\bar{c}$	6.3	6.7	7.8	5.0	5.3	6.2
$b\bar{b}$	5.1	5.5	6.3	4.1	4.3	5.0

bounds on rare decays of τ, hadrons or heavy quarks. Tensor operators were not considered, and some of the operators, such as $\bar{c}u\bar{\mu}\tau$, were completely unbounded.

In this article, we consider $\mu\tau$ production at hadron colliders via these operators. Tables 3 and 4 list the new physics scales that are accessible at the Tevatron and the LHC, respectively. Due to much smaller backgrounds, both the LHC and Tevatron are more sensitive to electronic τ decays than hadronic τ decays. For hadronic τ decays, the LHC receives an enhancement from the large invariant mass region and is more sensitive than the Tevatron. Since the backgrounds to electronic τ decays at the Tevatron are much smaller than those at the LHC, the Tevatron is more sensitive than the LHC to electronic τ decays. We found that at the Tevatron with 8 fb^{-1}, one can exceed current bounds for most operators, with most 2σ
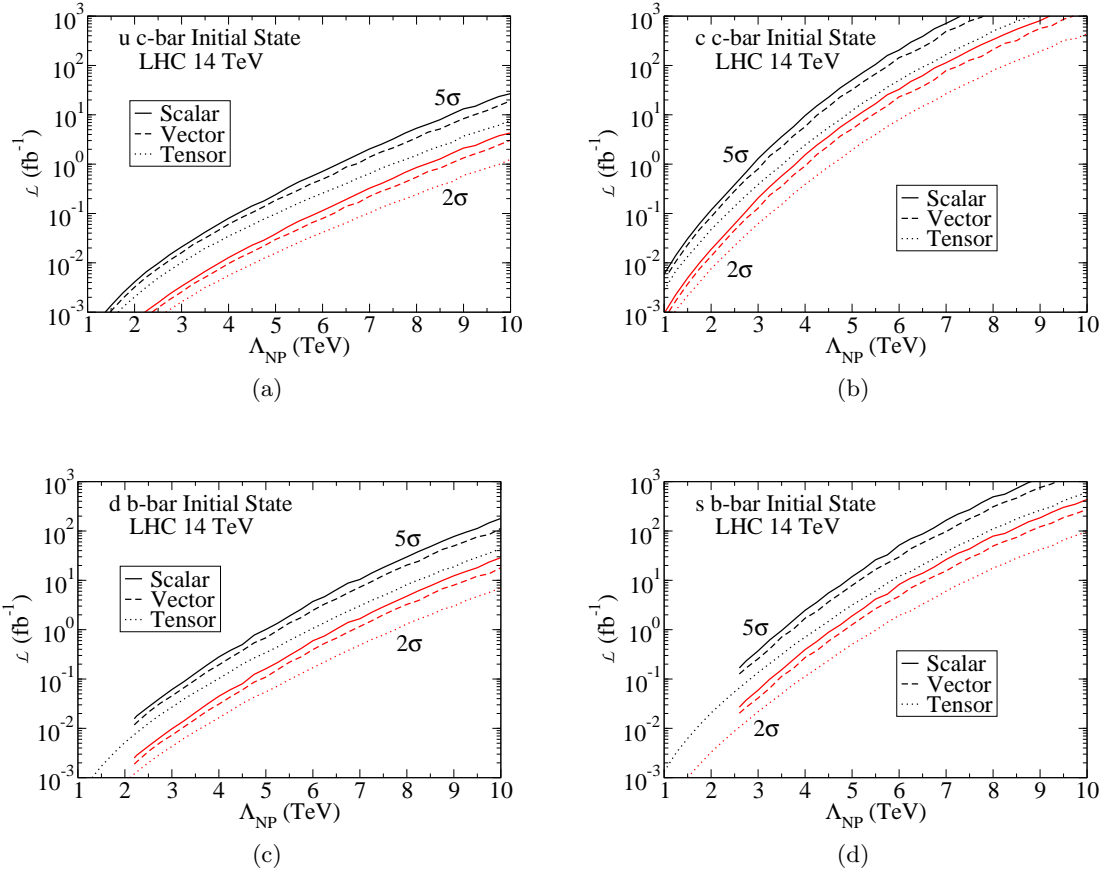
Figure 4: Luminosity at 14 TeV LHC needed for 2σ and 5σ observation of various new physics scales and electronic τ decay, (a) for the sensitivity for the $u\bar{c}$ initial state and (b) for the sensitivity needs for the $c\bar{c}$ initial state, (c) shows the sensitivity for the $d\bar{b}$ initial state, and (d) shows the sensitivity needs for the $s\bar{b}$ initial state. The lower bounds on the new physics scale were taken from BHHS.

sensitivities being in the $6 - 24$ TeV range. We find that at the LHC with 1 fb^{-1} (100 fb^{-1}) integrated luminosity, one can reach a 2σ sensitivity for $\Lambda \sim 3 - 10$ TeV ($\Lambda \sim 6 - 21$ TeV), depending on the Lorentz structure of the operator.

Acknowledgments

A. New Physics Bounds

Bounds from BHHS in TeV. The *'s indicate there are no bounds on the new physics scale and there are no bounds for the Tensor coupling.

Coupling type	1	γ_5	γ_μ	$\gamma_\mu\gamma_5$
$u\bar{u}$	2.6	12	12	11
$d\bar{d}$	2.6	12	12	11
$s\bar{s}$	1.5	9.9	14	9.5
$d\bar{s}$	2.3	3.7	13	3.6
$d\bar{b}$	2.2	9.3	2.2	8.2
$s\bar{b}$	2.6	2.8	2.6	2.5
$u\bar{c}$	*	*	0.55	0.55
$c\bar{c}$	*	*	1.1	1.1
$b\bar{b}$	*	*	0.18	*

B. Partial Wave Unitarity Bounds

Since the cross section from our higher-dimensional operators increases as s, it is necessary to determine the unitarity bound for $q\bar{q} \to \mu\tau$. The partial wave expansion for $a + b \to 1 + 2$ can be written as

$$\mathcal{M}(s,t) = 16\pi \sum_{J=M}^{\infty} (2J+1)a_J(s)d_{\mu\mu'}^J(\cos\theta)$$

where

$$a_J(s) = \frac{1}{32\pi} \int_{-1}^{1} \mathcal{M}(s,t)d_{\mu\mu'}^J(\cos\theta)d\cos\theta$$

and where $\mu = s_a - s_b$, $\mu' = s_1 - s_2$ and $J \leq \max(|\mu|, |\mu'|)$. The condition for unitarity is $|\Re(a_J)| \leq 1/2$.

It is straightforward to calculate the coefficients for the S,V,T operators. For example, for the scalar operator

$$\mathcal{M} = \frac{4\pi}{\Lambda^2}\bar{v}_{\lambda_1}(p_1)u_{\lambda_2}(p_2)\bar{u}_{\lambda_3}(p_3)v_{\lambda_4}(p_4)$$

one can just plug in the explicit expressions:

$$u_\lambda(p) \equiv \begin{pmatrix} \sqrt{E - \lambda|p|}\chi_\lambda(\hat{p}) \\ \sqrt{E + \lambda|p|}\chi_\lambda(\hat{p}) \end{pmatrix}$$

$$v_\lambda(p) \equiv \begin{pmatrix} -\sqrt{E + \lambda|p|}\chi_{-\lambda}(\hat{p}) \\ \sqrt{E - \lambda|p|}\chi_{-\lambda}(\hat{p}) \end{pmatrix}$$

where $\chi_+(\hat{z}) = \begin{pmatrix} 1 \\ 0 \end{pmatrix}, \chi_-(\hat{z}) = \begin{pmatrix} 0 \\ 1 \end{pmatrix}$. In the massless limit, this simply gives $a_0 = s/(4\Lambda^2)$ and so the unitarity bound gives $s \leq 2\Lambda^2$. For the vector case, $a_0 = 0$ and $a_1 = s/(6\Lambda^2$ giving the

unitary bound $s \leq 3\Lambda^2$. The tensor case gets contributions from both a_0 and a_1, and the stronger bound then applies.

References

[1] S. Fukuda, *et al.*, [Super-Kamiokande Collaboration], Phys. Rev. Lett. **85**, 3999 (2000); **86**, 5656 (2001); **82**, 1810 (1999); **81**, 1562 (1998); **81**, 1158 (1998); and T. Toshito, [Super-Kamiokande Collaboration], `hep-ex/0105023`.

[2] S. Fukuda, *et al.*, [Super-Kamiokande Collaboration], Phys. Rev. Lett. **86**, 5656 (2001); Q. R. Ahmad, *et al.*, [SNO collaboration], Phys. Rev. Lett. **87**, 071301 (2001). Q. R. Ahmad, *et al.*, [SNO Collaboration], Phys. Rev. Lett. (2002), `nucl-ex/0204008` and `nucl-ex/0204009`.

[3] D. Black, T. Han, H. J. He and M. Sher, Phys. Rev. D **66**, 053002 (2002) [arXiv:hep-ph/0206056].

[4] T. Han and D. Marfatia, Phys. Rev. Lett. **86**, 1442 (2001) [arXiv:hep-ph/0008141].

[5] K. A. Assamagan, A. Deandrea and P. A. Delsart, Phys. Rev. D **67**, 035001 (2003) [arXiv:hep-ph/0207302].

[6] U. Cotti, J. L. Diaz-Cruz, R. Gaitan, H. Gonzales and A. Hernandez-Galeana, Phys. Rev. D **66**, 015004 (2002) [arXiv:hep-ph/0205170]; J. L. Diaz-Cruz, D. K. Ghosh and S. Moretti, Phys. Lett. B **679**, 376 (2009) [arXiv:0809.5158 [hep-ph]].

[7] A. Brignole and A. Rossi, Phys. Lett. B **566**, 217 (2003) [arXiv:hep-ph/0304081].

[8] E. Arganda, A. M. Curiel, M. J. Herrero and D. Temes, Phys. Rev. D **71**, 035011 (2005) [arXiv:hep-ph/0407302].

[9] A. Azatov, M. Toharia and L. Zhu, Phys. Rev. D **80**, 035016 (2009) [arXiv:0906.1990 [hep-ph]].

[10] F. Deppisch, J. Kalinowski, H. Pas, A. Redelbach and R. Ruckl, arXiv:hep-ph/0401243.

[11] H. U. Bengtsson, W. S. Hou, A. Soni and D. H. Stork, Phys. Rev. Lett. **55**, 2762 (1985).

[12] D. Stump, J. Huston, J. Pumplin, W. K. Tung, H. L. Lai, S. Kuhlmann and J. F. Owens, JHEP **0310** (2003) 046 [arXiv:hep-ph/0303013].

[13] M. S. Carena *et al.* [Higgs Working Group Collaboration], Report of the Tevatron Higgs working group, arXiv:hep-ph/0010338.

[14] G. L. Bayatian *et al.* [CMS Collaboration], J. Phys. G **34**, 995 (2007). G. Aad *et al.* [The ATLAS Collaboration], arXiv:0901.0512 [hep-ex].

[15] P. Svoisky [D0 Collaboration], Nucl. Phys. Proc. Suppl. **189**, 338 (2009).

[16] B. Abbott *et al.* [D0 Collaboration], Phys. Rev. D **62**, 092004 (2000) [arXiv:hep-ex/0006011];
J. Piper [CDF Collaboration and D0 Collaboration], arXiv:0906.3676 [hep-ex].